Characterizing lead-rich particles in Beijing's atmosphere following coal-to-gas conversion: Insights from single particle aerosol mass spectrometry

Xiufeng Lian[1, 2], Yongjiang Xu[1], Fengxian Liu[3], Long Peng[4], Xiaodong Hu[5], Guigang Tang[6], Xu Dao[6], Hui Guo[7], Liwei Wang[8], Bo Huang[2], Chunlei Cheng[1], Lei Li[1], Guohua Zhang[9], Xinhui Bi[9], Xiaofei Wang[10], Zhen Zhou[1], Mei Li[1,*]

[1] College of Environment and Climate, Institute of Mass Spectrometry and Atmospheric Environment, Guangdong Provincial Engineering Research Center for On-line Source Apportionment System of Air Pollution, Jinan University, Guangzhou, 510632 PR China

[2] Guangzhou Hexin Instrument Co., Ltd., Guangzhou 510530, Guangdong, China

[3] Taiyuan University of Technology, Taiyuan 030024, PR China

[4] College of Ecology and Environment, Xin Jiang University, Urumqi 830046, PR China

[5] Jiangmen Laboratory of Carbon Science and Technology, Hong Kong University of Science and Technology (Guangzhou), Jiangmen 529100, PR China

[6] China National Environmental Monitoring Centre, Beijing 100012, PR China

[7] Hunan Province Environmental Monitoring Center, Changsha 410014, PR China

[8] Environment Emergency Monitoring and Accident Investigation Center, Jiaxing 314000, PR China

[9] State Key Laboratory of Organic Geochemistry and Guangdong Provincial Key Laboratory of Environmental Protection and Resources Utilization, Guangzhou Institute of Geochemistry, Chinese Academy of Sciences, Guangzhou 510640, PR China

[10] Department of Environmental Science and Engineering, Shanghai Key Laboratory of Atmospheric Particle Pollution and Prevention, Fudan University, Shanghai 200433, China

Correspondence to: limei@jnu.edu.cn

Abstract. Coal-to-gas (CTG) policies are important energy transformation strategies to address air pollution issues, but how well they improve atmospheric lead (Pb) pollution remains poorly understood. By the end of 2018, Beijing had achieved coal-free in urban and plain areas. The mixing state and atmospheric chemical processes of Pb-rich particles in Beijing were monitored using a single particle aerosol mass spectrometry (SPAMS) in 2019. Based on a large dataset of mass spectra, this study finds that the number fractions of Pb-rich particles, as well as two types of Pb-rich particles (K-Na-EC and K-OC) related to coal combustion during the heating period, show lower than those after the heating period. Based on concentration-weighted trajectory plots, the results indicate that lead aerosols mainly derive from the transmission of surrounding provinces. Lead nitrate is one of the important forms of lead in aerosol particles, most contributed by photo-chemical reactions in spring, fall, and winter. Due to nitrate decomposition during high temperatures, the aqueous reaction mechanism contributes more to lead nitrate in summer. These results improve our understanding of the seasonal distribution, formation mechanisms, and influencing factors of toxic Pb-containing particles after CTG.

1 Introduction

Lead (Pb), as one of the ubiquitous toxic metals, has been widely noted for its serious harm to human health (Cho et al., 2011; Grandjean and Herz, 2015; Lu et al., 2019; Schindler et al., 2021; Sommar et al., 2013). Pb-containing particles enter the lungs and blood of the human body through the respiratory tract, and accumulate in circulation within the body using blood as a carrier (Oberdörster et al., 2004); thus, they can severely damage DNA, kidney, and nervous system (Gu et al., 2018; Shtepliuk et al., 2018; Wani et al., 2015; Yedjou et al., 2016). Previous studies have suggested that no level of Pb in the human body is considered safe (Jakubowski, 2011; Rossi, 2008). Additionally, atmospheric Pb is also considered to contribute to climate modification as a cloud condensation nucleus (Cziczo et al., 2009; Ebert et al., 2011).

Pb enters the atmosphere through emissions from natural and anthropogenic sources. The Pb emission fluxes from anthropogenic sources are at least 1−2 orders of magnitude higher than those from natural sources (Komárek et al., 2008). Since the 1980s, atmospheric Pb has declined sharply due to leaded gasoline being phased out (Cho et al., 2011; Kristensen, 2015). Later, the decrease in airborne Pb emissions from automobiles increased the relative contribution of smelters, coal combustion, and waste incineration (Cai et al., 2017; Cho et al., 2011; Liang and Mao, 2015; Lu et al., 2019; Peng et al., 2020; Zhang et al., 2009; Zhao et al., 2017). Atmospheric Pb is primarily released during high-temperature processes due to condensation of its vapors and/or coagulation with existing particles (Csavina et al., 2014; Murphy et al., 2007). Lead production smelting processes and coal combustion processes emit PbS, PbO, and $PbSO_4$ into the atmosphere (Koukouzas et al., 2011; Sobanska et al., 1999; Tian et al., 2013; Yoshiie et al., 2013). The other two forms of lead compounds are $PbCl_2$ and $Pb(NO_3)_2$, which mainly come from the atmospheric aging process of Pb-containing aerosols (Schindler et al., 2021). $PbCl_2$ formed through the heterogeneous reaction between PbO and HCl during smelting combustion (Furimsky, 2000; Ohmsen, 2001) or waste incineration (Li et al., 2017; Moffet et al., 2008; Zhang et al., 2009). $Pb(NO_3)_2$ is generated from the chemical transformation of PbO and $PbCl_2$ in the atmospheric process (Moffet et al., 2008; Peng et al., 2020). These processes are crucial for Pb showed a significant negative impact on health because of the high solubility of $Pb(NO_3)_2$ (Bas et al., 2016; Bas and Kalender, 2016).

Coal combustion during winter heating is an important source of Pb-containing particles in Beijing, China (Li et al., 2012; Murphy et al., 2007; Peng et al., 2020). Since 2013, the government introduced a series of strict measures to advance the conversion of coal to clean energy. By the end of 2018, villages in Beijing's plain area have achieved coal-free transformation (Wang et al., 2021). Urban clean fuel centralized heating has been completed. Therefore, the elimination of coal combustion thus provided a valuable opportunity to fully understand the contribution of coal combustion sources to atmospheric Pb and the atmospheric Pb sources previously masked by coal combustion sources. However, there is still a lack of research on the source, transport, and evolution process of Pb particles after CTG.

Traditional atmospheric Pb data are off-line collected by Particle Analysis by Laser Mass Spectrometry (PALMS), Transmission Electron Microscope (TEM), and Scanning Electronic Microscopy (SEM) (Murphy et al., 2007; Schindler et

al., 2021). Off-line techniques are useful for providing accurate mass concentration values for Pb but show poor temporal resolution. More recently, mass spectrometry-based online techniques such as single-particle mass spectrometer (SPMS)(Lu et al., 2019) have been favored. Although these techniques are typically not quantitative, they provide information on the sources and mixing state of Pb in real time. This information is critical to understanding the atmospheric transport and aging processes of Pb. Lu et al. (2019) analyzed the mixed state of Pb-containing particles monitored by SPMS and found that the sources of particulate Pb in Guangzhou, China include coal combustion, waste incineration, vehicle exhaust, industrial process, and dust. Moffet et al. (2008) used a SPMS to monitor the diurnal variation characteristics of Zn or Pb single particles in industrial areas in Mexico and found that Zn or Pb chloride converted to metal nitrate began each day at ~7 am.

To better understand the mixing state, source, and atmospheric evolution process of atmospheric Pb after CTG, we investigate Pb-containing individual particles with a high time resolution in the atmosphere of urban Beijing from spring to winter in 2019. The three specific goals are to: 1) compare the differences of Pb-rich particles between heating and non-heating periods; 2) investigate the sources and mixing state of Pb-rich particles after CTG; and 3) expound the diurnal and seasonal variation characteristics of particulate lead nitrate and its possible formation mechanism of atmospheric Pb after CTG.

2 Field measurements

2.1 Data Collection

The sampling site was located in Beijing at the China National Environmental Monitoring Centre (40.05° N, 116.43° E; 40 m a.s.l.) in Beijing. Sampling was conducted during spring (March 9–April 8, 2019), summer (June 16–July 9, 2019), fall (September 15–October 16, 2019), and winter 2019 (December 15, 2019–January 15, 2020). The central heating period in Beijing is from 00:00 on November 15th to 23:00 on March 15th. Sampling in spring and winter covers a central heating period, respectively. Local meteorological parameters, including RH, temperature (T), wind speed, wind direction, and the concentrations of NO_2, SO_2, O_3, and $PM_{2.5}$ from 2019 to 2020 are provided by the China National Environmental Monitoring Centre (**Table S1**).

This study used a single particle aerosol mass spectrometer (SPAMS, Hexin Analytical Instrument Co., Ltd., Guangzhou, China) to monitor the size and chemical composition of aerosol particles with a vacuum aerodynamic diameter of 0.1–2.0 micrometers (d_{va}). Ambient particles are separated by a $PM_{2.5}$ cyclone separator and dried with silica gel before entering the single particle aerosol mass spectrometer. The detailed setup and mechanisms of the SPAMS have been described elsewhere (Li et al., 2011). Briefly, aerosol particles were introduced into the SPAMS through a 0.1 mm critical orifice at a flow rate of 80 ml min^{-1}. Then, they were focused and aerodynamically sized by two continuous diode Nd:YAG laser beams (532 nm), followed by desorption/ionization by a pulsed laser (266 nm) that was triggered exactly based on the time of flight during the sizing. The positive and negative fragments generated were then detected using a time-of-flight spectrometer.

2.2 Data Analysis

Data analysis is performed by importing single-particle size and mass spectra into MATLAB (The MathWorks, Inc.) using the Continuation Core (COCO; version 3.0) toolkit. A total of ~650 000 to ~3 400 000 particles with both positive and negative ion mass spectra were obtained by the SPAMS. Among them, around 20 000 to 140 000 (2.8−4.4%) Pb-containing particles were identified with ion signals > 5 (> 3 times the noise level) at mass-to-charge ratios (m/z) of 206, 207 and 208. Pb-rich particles are defined as particles with a relative intensity of ^{208}Pb greater than 5% of the total intensity in a mass spectrum, which is the same criterion that has been used in previous online Pb single-particle studies (Cai et al., 2017; Peng et al., 2020; Zhang et al., 2009). We measured 8 034−23 941 Pb-rich particles, accounting for 0.7−1.2% of all detected particles and 16.0−44.5% of Pb-containing particles (**Table 1**). During the sampling period, there was a significant correlation between the number of Pb-containing particles and Pb-rich particles in all the detected particles, with correlation coefficients $r > 0.85$ and $p<0.01$. Moreover, the size distribution characteristics of Pb-containing particles and Pb-rich particles are similar (**Fig. S1**). The correlation between Pb-containing particles and Pb-rich particles in winter ($r = 0.47$, $p<0.01$) is much lower than that in other seasons. The number fractions of Pb-rich particles decreased significantly, accounting for only 16% of Pb-containing particles in winter, which is 40% lower than that in other seasons. Previous results showed that Pb-rich particles typically undergo less aging process than non-Pb-rich particles (Zhang et al., 2009). Thus the weaker correlation in winter may be related to the accumulation of non-Pb-rich particles after the conversion of Pb-rich particles to non-Pb-rich particles caused by poor diffusion conditions. Therefore, this study focuses on Pb-rich particles with higher relative strength fractions of Pb than that in Pb-containing particles, which are more likely to imply higher lead concentrations in individual particles and have relatively simple chemical histories.

The screened Pb-rich particles were subsequently analyzed using an adaptive resonance theory-based neural network algorithm (ART-2a) (Song et al., 1999), with a vigilance factor of 0.75, a learning rate of 0.05, and 20 iterations. To analyze the source of Pb-rich particles, approximately 95% of the particles were classified by ART-2a and manually classified into six types based on positive spectral signal intensity. The mixed state of lead, nitrate, and other ions is identified by whether the marker ions of lead and other ions are in the same single particle spectrum. They are named potassium-sodium (K-Na), K-Na mixed with Fe (K-Na-Fe), K-Na mixed with Cu (K-Na-Cu), K-Na mixed with Zn (K-Na-Zn), K-Na mixed with elemental carbon (K-Na-EC), and potassium mixed organic carbon (K-OC). The remaining particles were classified as "Others". The average mass spectra for the main Pb-rich particle types are shown in **Fig. 1**.

The definition of lead nitrate (Pb-N) particles in this study is the particles mainly composed of nitrate in the negative spectrum of Pb-rich particles, and the nitrate peak area is strongly correlated with lead (Peng et al., 2020). Although this method has limitations in fully capturing the variability or total content of lead nitrate, it does not impact the accuracy of the analysis results of lead nitrate in this study. There are significant correlations exist between Pb-N particles and Pb-rich

particles mixed with nitrate *(r = 0.84−0.96, p < 0.01)*, *ensuring that the observed trends and relationships remain robust and*

reliable. In this study, the average mass spectrum and digital spectrum of Pb-N particles are shown in **Fig. 2** and **Fig. S2−3**. Pb-N particles mainly consist of nitrate in the negative spectrum, and iron, sodium, potassium, and a small amount of organic compounds in the positive spectrum. There is significant correlation *(r = 0.82−0.98, p < 0.01)* between the total peak area of nitrates (sum peak area of *m/z* −46 and −62) and the total peak area of lead (sum peak area of *m/z* 206, 207, and 208) in Pb-N particles(**Fig. S4**). The weak correlation between nitrates and sodium, potassium, and iron *(r = 0−0.42, P < 0.01)* are also found. Thus, these Pb-N type particles are also most likely represented as $Pb(NO_3)_2$ in this study.

2.3 Concentration Weighted Trajectory (CWT) model

The CWT model was applied to localize potential source areas affecting aerosol particles at a receptor site (Watson et al., 2008). In this procedure (Equation R1), each grid cell gets a weighted concentration obtained by averaging sample concentrations that have associated trajectories that crossed that grid cell as follows (Hsu et al., 2003):

$$C_{ij} = \frac{1}{\sum_{l=1}^{M} \tau_{ijl}} \sum_{l=1}^{M} C_l \tau_{ijl}) \qquad (R1)$$

$$W(i,j) = \begin{cases} 1.0 & (3n_{ave} < n_{ij}) \\ 0.7 & (1.5n_{ave} < n_{ij} < 3n_{ave}) \\ 0.4 & (n_{ave} < n_{ij} < 1.5n_{ave}) \\ 0.2 & (n_{ave} < n_{ij}) \end{cases} \qquad (R2)$$

C_{ij} is the weighted average concentration in a grid cell (i, j), l is the index of the trajectory, M is the total number of trajectories, C_l is the concentration observed on the arrival of trajectory l, τ_{ijl} is the time spent in the ij^{th} cell by trajectory l. $W(i,j)$ is the weighting function and n_{ij} is the number of endpoints through the ij cell. The weighted concentration fields show concentration gradients across potential sources. The back-trajectory analyses were conducted with the HYSPLIT4 model from the U.S. National Oceanic and Atmospheric Administration (Draxler and Rolph, 2003), with the arrival altitude and calculation time set at 100 m and 72 h, respectively.

3 Results and discussions

3.1 Mixing state and sources of Pb-rich particles

K-Na-EC particles can be distinguished from the other Pb-rich particles by their distinct EC cluster ions with C_n^+/C_n^- (n: 2–5) in the mass spectra (**Fig. 1**), accounting for 1.5–8.9% of all the detected particles (**Table 1**). The spectral characteristics of K-Na-EC particles in this study are similar to those of Pb-EC/OCEC-rich particles in previous studies of Pb-containing single particles, which are confirmed to be most likely attributed to combustion emissions, especially from coal combustions (Cai et al., 2017; Peng et al., 2020). The number fractions of Pb-EC particles during the heating period was ~5−10%, while before the heating period, it was ~1−2% in the winter of 2014 (Peng et al., 2020). EC particles are directly emitted from sources such as vehicle exhaust, industrial processes, and biomass burning due to incomplete combustion of organic species (Tiwari et al., 2013). Pb-containing particles from vehicle combustion are often coated with semi-volatile organic carbon species, and K-Na-EC from diesel truck exhaust mostly coexists with phosphate (Amann and Siegla, 1982; Lu et al., 2019). In this study, K-Na-EC particles contain very weak OC fragments such as *m/z* 51 $[C_4H_3]^+$ and 63 $[C_5H_3]^+$), and the number

fractions of phosphate (m/z –79 [PO_3]⁻) in K-Na-EC particles accounted for only 10.4%. In addition, Pb is only a minor component in particles from biomass burning (Bi et al., 2011; Hudson et al., 2004; Murphy et al., 2007). Considering these factors, the K-Na-EC particles in this study are most likely from coal combustion.

OC particles exhibit spectral variation with strong m/z 39 [K]⁺and weak OC fragments (m/z 37 [C_3H]⁺ and 51 [C_4H_3]⁺), accounting for 1.0–4.4% of all the detected particles. The significant correlation between K-OC and K-Na-EC particles (r = 0.58, p < 0.01; **Fig. S5(a)**) indicates that they may be homologous (Cai et al., 2017; Lu et al., 2019). The K-Na-EC and KOC particles showed a similar distribution in that the number fractions decreased with increasing d_{va}, and represented the highest fraction (46.4–71.4%) in the size range of 0.1–0.4 μm (**Fig. S6**). Additionally, K-Na-Cu particles show similar size distribution characteristics with K-OC and K-Na-EC particles, accounting for 1.2–3.3% of all the detected particles. K-Na-Cu particles are identified by the intense ion signals from Cu (m/z 63/65 [Cu]⁺) and phosphate, with a peak particle size distribution of 0.5–0.6 μm. They are probably from industrial coal combustion, as the mass spectrum and particle size distribution characteristics of K-Na-Cu particles are similar to those of Pb-containing particles released from industrial coal combustion (Lu et al., 2019).

K-Na-Fe particles exhibit spectral variation with strong a dominant iron signal at m/z 56 [Fe]⁺ and a weaker signal from its natural isotope m/z 54 [Fe]⁺ in the positive spectrum. K-Na-Zn is recognized by a strong signal at m/z 64 [Zn]⁺ and a weaker signal from its natural isotope m/z 66 or 68 [Zn]⁺ in the positive spectrum. Unlike the particle types mentioned earlier, the negative spectra of K-Na-Fe and K-Na-Zn particles contain strong nitrate (m/z –46 [NO_2]⁻ and –62 [NO_3]⁻) peaks, but the sulfate (m/z –97 [HSO_4]⁻) peaks are very weak. They are distributed in larger particle sizes (>0.5 μm), indicating that they are more aged than those from combustion. K-Na-Fe and K-Na-Zn particles account for 4.9–6.8% and 0.1–0.9% of all the detected particles, respectively. K-Na-Fe and K-Na-Zn particles are highly likely to originate from industrial processes, such as metal smelting processes. Industrial emissions of Pb are mainly from nonferrous metal smelting, usually mixed with Fe and/or Zn in the particle phase (Batonneau et al., 2004; Lu et al., 2019; Moffet et al., 2008; Tian et al., 2015). Lu et al., (2019) demonstrated that K-Na-Zn particles in environmental aerosols are most likely to originate from industrial processes by comparing atmospheric LCP mass spectra with authentic Pb emission source mass spectra. Previous research has shown that the number fractions of the Pb-rich particles mixed with Fe and Zn significantly decrease during the heating season, with decreases of 8% and 6%, respectively (Peng et al., 2020).

K-Na particles exhibit spectral variation with strong m/z 39 [K]⁺and m/z 23 [Na]⁺ in the positive spectrum, and strong nitrate in the negative spectrum. K-Na particles are the most abundant particle type in environmental aerosols, accounting for 78.4–84.3% of all detected particles. The vast majority of K-Na particles are emitted from non-coal combustion sources (Murphy et al., 2007; Tian et al., 2015). K-Na particles are not correlated with the number fractions of K-Na-EC and K-OC particles. The relative number fractions of K-Na particles decreased significantly in the heating season. Particles of K-Na mixed with Li (m/z 7 [Li]⁺), which may come from coal combustion fly ash (Furutani et al., 2011; Guazzotti and S., 2003; Liu et al., 1997), account for only 3.5% (by number) of all K-Na particles. Most (83.1–97.8%) of K-Na particles are distributed in the particle size larger than 0.5 μm, same as K-Na-Zn and K-Na-Fe particles. A significant correlation (r = 0.61, p < 0.01; Fig.S7(b)) between the number fractions of K-Na and K-Na-Fe is also observed. These results suggest that K-Na and K-Na-Fe particles have the same primary sources and undergo similar atmospheric aging processes. We speculate the major primary sources of Pb in Beijing have changed from combustion processes and the iron/steel industry after CTG.

3.2 The reduced contribution of local coal combustion to Pb-rich particles after coal-to-gas

The variation characteristics of Pb-rich particles and various types of Pb-rich particles during the heating period (HP) and after HP in spring 2019 are shown in **Fig. 3**. The average number fractions of Pb-rich particles during HP is 28.6% lower than that after HP, and this trend of lead nitrate particles (42.2%) is more significant (**Fig. 3(b)**). The maximum hourly

number fractions of Pb-rich and Pb-N particles after HP are usually one to two twice that during HP (**Fig. 3(a)**). This is a significant decrease compared to double the average and maximum hourly number fractions of Pb-rich particles during the past coal-fired centralized heating period in Beijing (Peng et al., 2020). In addition, during the heating period, the concentrations of pollutants (PM$_{2.5}$, NO$_2$, SO$_2$, CO, and O$_3$) are also lower than those during non-heating periods (**Fig. S7(a)**). The relative peak area of Pb in Pb-rich particles in the heating season including spring and winter is about 15% lower than that in non-heating season (**Fig. S7(b)**). Previous studies on the impact of coal-to-gas conversion policies on air quality have shown that this policy led to PM$_{2.5}$, SO$_2$, and other air quality parameters significantly improved. On average, the "coal-to-gas" policy reduced SO$_2$, NO$_2$, PM$_{10}$, PM$_{2.5}$, and CO by 12.08%, 4.89%, 13.07%, 11.94%, and 11.10% per year from 2014 to 2018 in Beijing, respectively (Liu et al., 2020). Our results provide evidence that the "coal-to-gas" policy has also effectively improved the pollution of Pb-containing aerosols.

We note that the total relative number fraction of K-Na-EC and KOC particles associated with coal combustion sources doubled during the HP compared to the non-heating period (**Fig. 3 (c)**). In winter, the total relative number fraction of K-Na-EC and KOC particles is more than twice that of non-heating seasons in summer and fall (**Fig. S8**). Sampling in winter is 25 days longer than in spring during the heating period, and the total relative number fraction of K-Na-EC and KOC particles is 60% higher than in spring. To identify the potential sources for the Pb-rich particles after CTG, the concentration-weighted trajectory (CWT) plots from spring to winter are analyzed (**Fig. 4**). The number of high-weighted cells in the web version presented the potential major source areas. The potential source area of atmospheric Pb is mainly dominated by external transport and exhibits seasonal variation characteristics. Pb-rich particles are mainly contributed by eastern Inner Mongolia, the central region of Liaoning Province, and at the junction of Anhui Province, Shandong Province, and Henan Province during spring. The high-value areas during summer and fall are mainly distributed in the eastern part of Shandong Province and Tianjin, as well as the western part of Liaoning Province. The potential winter source areas are distributed in the long-distance transmission of air masses from eastern Mongolia and the northern regions of Tianjin and Hebei Province. Previous research results have shown that on average 45% of Pb in PM$_{2.5}$ in urban Beijing was transported (Cai et al., 2017). It is noticeable that lead smelters and metal refining plants are widely distributed in this area with rich mineral resources (Cai et al., 2017; Liu et al., 2018; Tian et al., 2015). These regions are also the regions with higher lead emissions in China in 2020 (Tong et al., 2024).

3.3 Characteristics of size and mixing state during HP and after HP after coal-to-gas

The mixed state with anions is important fundamental data for further understanding the form of lead in environmental aerosols. In this study, about 60% of the Pb-rich particles are found to mixed with chloride and oxygen. This proportion remain consistent across the heating and non-heating periods in spring, as well as the heating period in winter (**Fig. 5**). However, the mixing ratio of Pb-rich particles with sulfate is about 10% higher during the spring heating period compared to the non-heating period. This increase is likely influenced by the sulfur dioxide concentrations (**Table S1**). After coal-to-gas conversion, the mixing state of lead in spring and winter are more complex than in summer and fall, with the number fractions of lead mixed with sulfate and chloride salts doubling compared to summer and fall.

Additionally, previous research has shown that the main forms of lead in aerosol particles include lead oxide, lead chloride, lead sulfate, and lead nitrate (Cai et al., 2017; Lu et al., 2019). In this study, almost all lead are mixed with nitrate, which is much higher than its mixing with sulfate, chlorine, and oxygen. More than 97% of Pb-rich particles are mixed with nitrate, while only 22−64% of Pb-rich particles are mixed with sulfate, chlorine, or oxygen. As shown in **Fig. S9**, the number fractions of Pb-N particles rises with increasing particle size, with over 85% of these particles found within the size range of 0.5 to 1.0 μm. This distribution suggests that the majority of lead nitrate originates from the secondary formation of Pb-containing particles during their transport. The number fractions of Pb-N particles in Pb-rich particles are 17.1−39.1% from spring to winter (**Table 1**). Among them, the number fractions of Pb-N particles are higher in summer and fall than

those in spring and winter. However, this result is inconsistent with the distribution characteristics of high nitrate levels in winter and lower nitrate levels in summer. To unravel this mystery, we further explore the possible formation mechanism of lead nitrate in the next section.

3.4 The possible formation mechanism of $Pb(NO_3)_2$ in the particle after coal-to-gas

Except for summer, the number fractions of Pb-N particles are higher during the day and lower at night, with high values mainly distributed between 10:00 and 15:00 (**Fig. 6**). In spring, Pb-N particles account for the lowest amount of all detected particles from 22:00 to 00:00, with an average of about 0.1%. After 00:00, the number fractions of Pb-N particles increase gradually until 9:00−15:00, and the number fractions of Pb-N particles increase to 0.3%, and then slowly decrease. The peak number fractions of Pb-N particles in fall lags behind that in spring by about two hours. It starts to rise rapidly at 10:00 in the morning and rises from 0.3% to 0.8% in three hours. After 14:00, it slowly drops to ~0.3% at 21:00, and fluctuates slightly between 0.2−0.3% from 22:00 to 10:00 the next day. The number fractions of Pb-N particles in winter with time is similar to that during fall, but the difference between the high value in daytime and other times is small, only 0.07%. In Mexico City aerosols, the conversion of lead chloride to lead nitrate occurs between 7:00−21:00 and peaks at 12:00−2:00 due to the effective formation of gaseous HNO_3 after sunrise (Moffet et al., 2008). Furthermore, the number fractions of Pb-N particles are slightly higher on sunny days than on non-sunny days in spring and winter (**Fig. 7**). Ozone, which reflects the activity of photochemical reactions, is significantly higher on sunny days than on non-sunny days, with an average value of 1.7−71.0% higher from spring to winter (**Fig. S10**). In particular, the low number fractions (~0.2%) of Pb-N particles are from 12:00 to 23:00, and the high value (~3.5%) is from 00:00 to 11:00 in summer. Previous results have shown that $Pb(NO_3)_2$ did not show any significant diurnal variation, both daytime and nighttime atmospheric processes contributed to the observed $Pb(NO_3)_2$ (Peng et al., 2020). These results support the importance of photo-oxidation for the formation of nitric acid and lead nitrate and highlight the seasonal differences in the formation process of lead nitrate.

Previous studies revealed that NO_2, RH, and T can affect the formation of lead nitrate in atmospheric aerosols. As a precursor of nitrate, NO_2 participates in the formation of lead nitrate both during the day and at night. A significant positive correlation ($r = 0.88$, $p < 0.01$) between the RH of nitrate and NO_2 was observed (Peng et al., 2020). Temperature, relative humidity, and light intensity indirectly affect the formation of lead nitrate by influencing the formation of nitrate. As suggested by previous studies, the heterogeneous hydrolysis of N_2O_5 under high RH plays a crucial role in particulate nitrate formation and significantly contributed to the elevated fine nitrate during nighttime (Zhang et al., 2017). Solar radiation affects the formation of OH radicals, and OH radicals are oxidants that transform NO_2 into HNO_3, so a high concentration of OH radicals is conducive to the formation of HNO_3. At the same time, higher temperature is also conducive to NO_2 and OH reactions (Slater et al., 2019). Specifically, the number fractions of Pb-N particles decreases with increasing T, especially when the temperature exceeds 30 ℃, which may be an indirect result of the decomposition of nitrate particles caused by high temperature (Song et al., 2019; Luo et al., 2020). Lead nitrate abundance begins to increase at sunrise and peaks at 12:00−2:00 (Moffet et al., 2008), consistent with the diurnal variation in temperature and light intensity. In this study, the number fractions of Pb-N particles increased with the increase of temperature between −10 ℃ and 30 ℃, and decreased with the increase of temperature above 30 ℃ (**Fig. 8**).

With the increase of NO_2, the number fractions of Pb-N particles decreased significantly in summer but did not change significantly in other seasons. The effect of NO_2 on the formation of lead nitrate is limited by RH. The relative intensity of nitrate exceeded 12% in most situations when the RH was higher than 60%, while the relative intensity of nitrate reached a maximum of 21% with RH above 80% (Peng et al., 2020). The decreased number fractions of Pb-N particles slightly with the increase of RH. This is inconsistent with the result that high RH promotes the formation of lead nitrate(Peng et al., 2020). It is important to note that this does not imply high RH inhibits the formation of lead nitrate. Instead, the observed trend may be influenced by the stronger impact of photo-chemical oxidation reactions, which are enhanced by high T and low RH

during the day, compared to the aqueous-phase reactions favored by high RH in the formation of lead nitrate.

Lead nitrates in atmospheric aerosols are generated by heterogeneous reactions of lead chloride or lead oxide with NO_2 or by aqueous reactions with nitric acid (Moffet et al., 2008; Peng et al.,2020). Primary emissions of $PbCl_2$ particles underwent heterogeneous transformations into nitrate particles as soon as the photochemical production of nitric acid (Moffet et al., 2008). Peng et al. (2020) used a SPAMS to study the transport and aging mechanism of lead in the winter atmosphere of Beijing before "coal-to-gas". The study included heating and non-heating periods, and the results emphasized the importance of heterogeneous hydrolysis during the heating period before "coal-to-gas" on the formation of $Pb(NO_3)_2$. The results of this study show that after the implementation of the coal-to-gas policy, the formation of lead nitrate in aerosols may shift from aqueous reaction dominance to photochemical reaction dominance in winter.

3.5 Uncertainties and Limitations

Although promising results and good comparisons are obtained from the analysis of particle size, particle number, and mixing state monitored by SPAMS, there are some uncertainties and limitations in this study. First, due to its lower detection efficiency at smaller sizes, we may underestimate Pb abundance on small particles. Secondly, we overlook the matrix effect, which affects the collection efficiency of SPAMS for different components. Despite the potential uncertainties discussed earlier, the strong correlation ($r = 0.58-0.70$; $p < 0.01$) between the counts of all detected particles and $PM_{2.5}$ concentrations indicates that these uncertainties did not significantly affect the results.

A limitation or bias of this study is the use of RPA spectral data in these qualitative individual masses, rather than absolute mass concentrations of lead. It should be noted that due to various uncertainties caused by laser ionization, such as matrix effects and incomplete ionization, laser ablative based SPAMS are still very challenging in providing quantitative information (Jeong et al., 2011; Healy et al., 2013; Zhou et al., 2016). Although different at the individual particle level, RPA is still a good indicator for studying the atmospheric processing and mixing state of various particle types, including Pb-containing particles (Moffet et al., 2008; Zauscher Et al., 2013; Peng et al., 2020). In this study, while we cannot quantitatively assess the impact of CTG policies on reducing lead levels in aerosols, our findings successfully reveal distinct characteristics of Pb-rich particles in the ambient atmosphere. This provides a valuable qualitative and semi-quantitative understanding of how Pb-rich particles evolve following the implementation of CTG policies. Future work should target a quantitative understanding of Pb concentration variations in aerosols and atmospheric evolution processes of Pb such as photo-oxidation.

Another limitation is the relatively short sampling time (6 days) during the spring heating period, which may introduce deviations in the mean values and assessment of the number fractions of Pb-rich particles, potentially affecting the representativeness of the data. However, the physical and chemical characteristics such as particle type and mixing state of Pb-rich particles during heating periods in both spring and winter show strong similarities (Fig. 5 and Fig. S8). This suggests that the short sampling time in spring heating season does not significantly compromise the accuracy of data results. Nonetheless, future studies could extend the sampling duration during heating periods to enhance the representativeness of the results.

4 Conclusions and implications

We studied the sources, mixing states, and seasonal variations of lead particles in the urban atmosphere of Beijing after coal-to-gas conversion, with a focus on the formation mechanism of toxic lead nitrate particles. K-Na-EC and K-OC particles are associated with coal combustion, and K-Na, K-Na-Fe, K-Na-Zn particles tend to come from iron/steel industries. Our results show that the contribution of coal combustion to atmospheric Pb decreases significantly after CTG, and the iron/steel industries become the most important emission source. The atmospheric Pb in Beijing's urban area is mainly transmitted from surrounding provinces such as Mongolia Province, Hebei Province, Liaoning Province, Anhui Province,

and Shandong Province. Almost all lead are mixed with nitrate, which is much higher than its mixing with sulfate, chlorine, and oxygen. The number fractions of Pb-N particles in Pb-rich particles are 17.1−39.1% from spring to winter, which is about twice as high in summer and fall as in spring and winter. The diurnal variation of number fractions of Pb-N particles show obvious seasonal difference. Results from this study show that the gas phase photo-oxidation contributed a lot to the formation of lead nitrate particles, especially in spring and fall.

Our results provide observational evidence for the effect of CTG policy on the reduction of Pb. This broadens the understanding of CTG to improve air quality, provides a scientific basis for a more accurate assessment of the comprehensive effect of CTG policies on air quality improvement (Liu et al., 2020). Since there is considerable debate regarding the atmospheric chemistry of Pb (Moffet et al., 2008; Peng et al., 2020), our findings further emphasize the importance of photochemical reactions and clarify their seasonal differences in the formation process of lead nitrate. Consider that a series of CTG policies have been implemented in Beijing,Tianjin, and 26 other cities in Hebei, Shanxi, Shandong, and Henan provinces) (https://www.gov.cn/xinwen/2017-12/20/content_5248855.htm), the research methods and conclusions of this study can also be extended to these cities.

Supplement. Supporting information includes ten figures (Fig. S1-S10), and one table (Table S1) related to the manuscript.

340

Data availability. The observational data including SPAMS and meteorological parameters used in this study are available from corresponding authors upon request (limei@jnu.edu.cn).

Author contributions. ML designed the research with input from XW, XB, GZ, and ZZ. YX, GT, and XD collected samples.

345   XL processed data and wrote the manuscript. FL, PP, XH, HG, and LW had an active role in supporting the sampling work. BH, CC, and LL had an active role in supporting the writing-original work. All authors contributed to the discussions of the results and refinement of the manuscript.

Competing interests. The authors declare that they have no conflict of interest.

350

Financial support. This study is supported by the National key research and development program (2023YFC3705502), the National Natural Science Foundation of China (Grant No. 42407355), Special Fund Project for Science and Technology Innovation Strategy of Guangdong Province (Grant No. 2019B121205004), Guangdong Foundation for Program of Science and Technology Research (Grant No. 2020B1212060053), State Environmental Protection Key Laboratory of Monitoring

355   for Heavy Metal Pollutants (Grant No. SKLMHM202325).
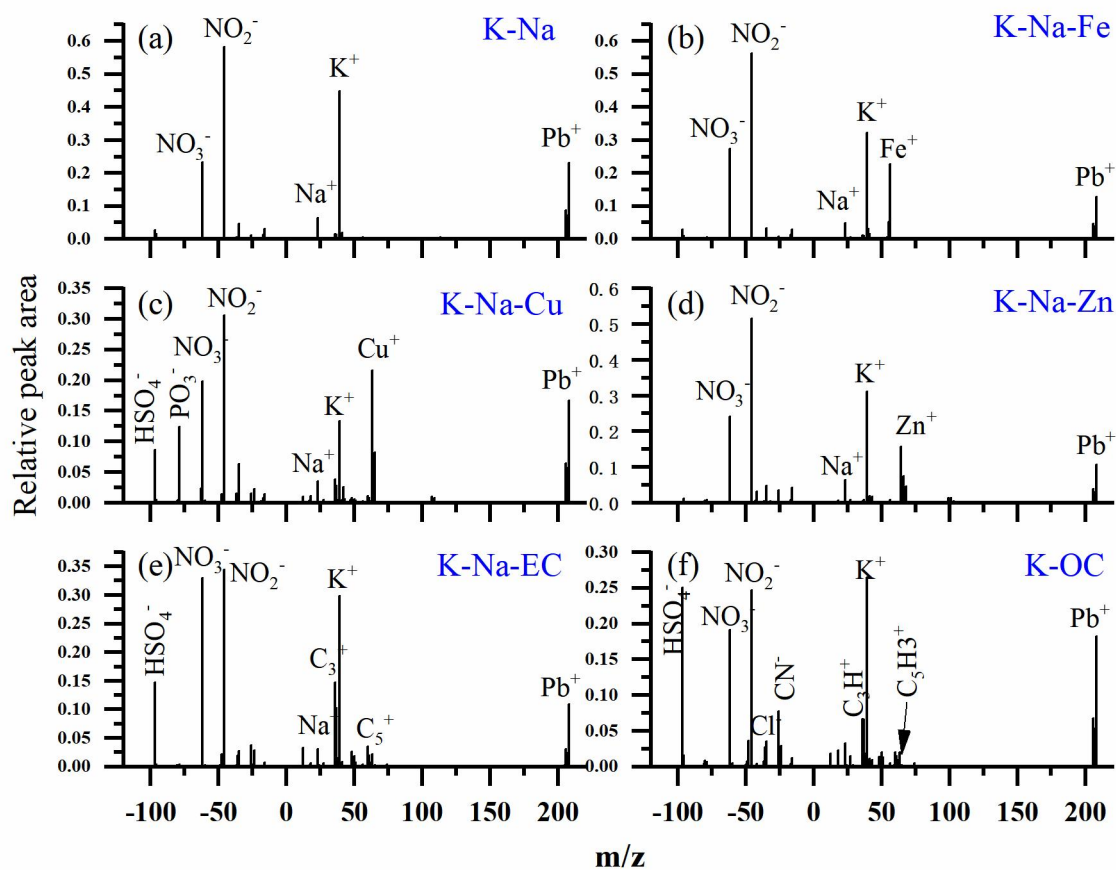
Figure 1. Average mass spectra for the main Pb-rich particle types.
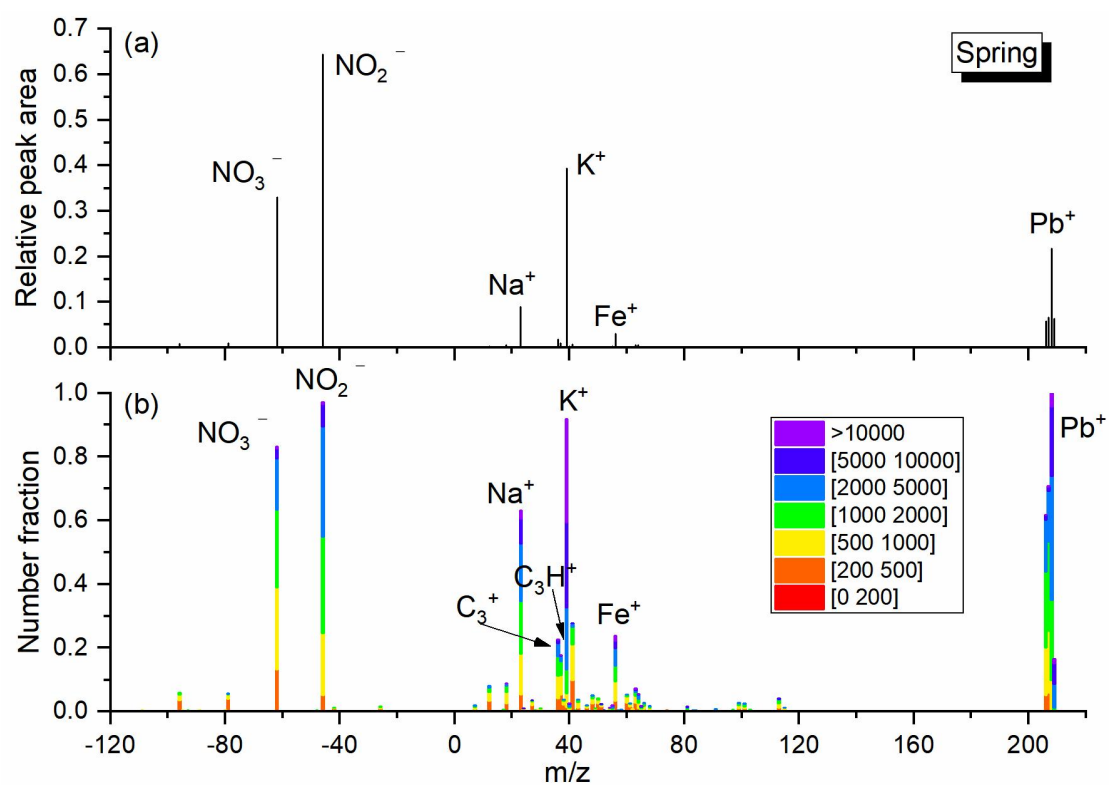
Figure 2. The average mass spectrum and digital spectrum of lead nitrate particles during spring.
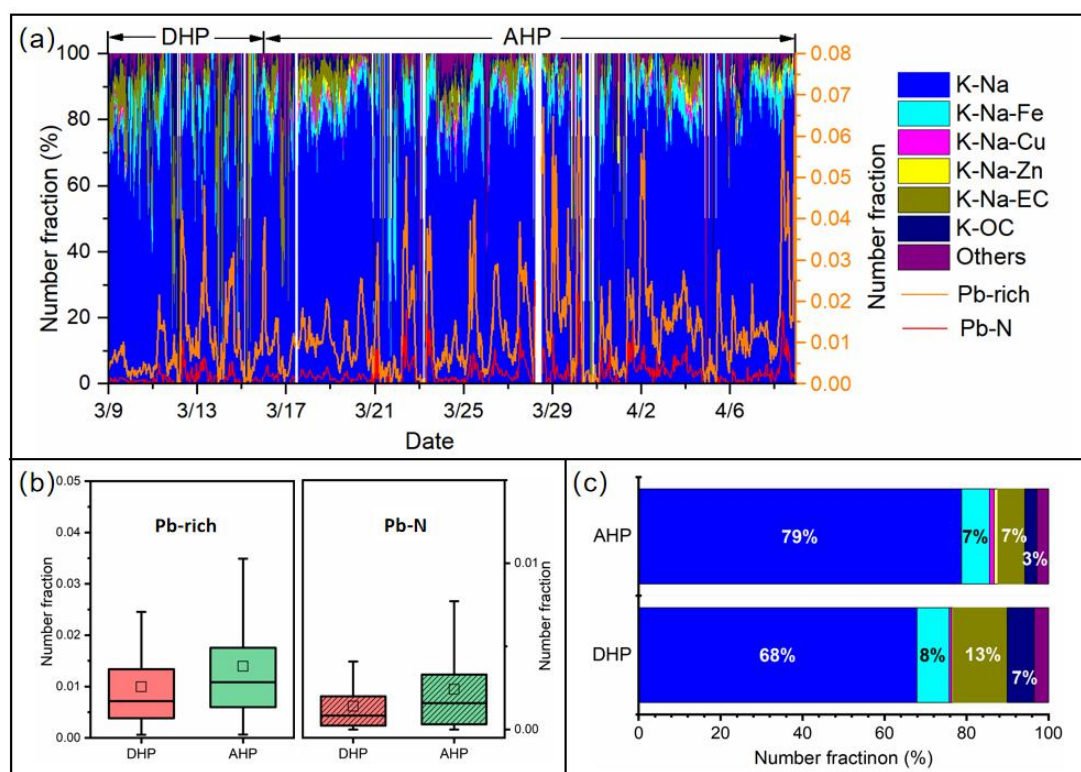
Figure 3. The time series of the main Pb-rich particle type particles (a), the number fractions of Pb-rich and Pb-N particles (b), and the relative abundance of seven types particles (c) during (DHP) and after the heating period (AHP) in spring.
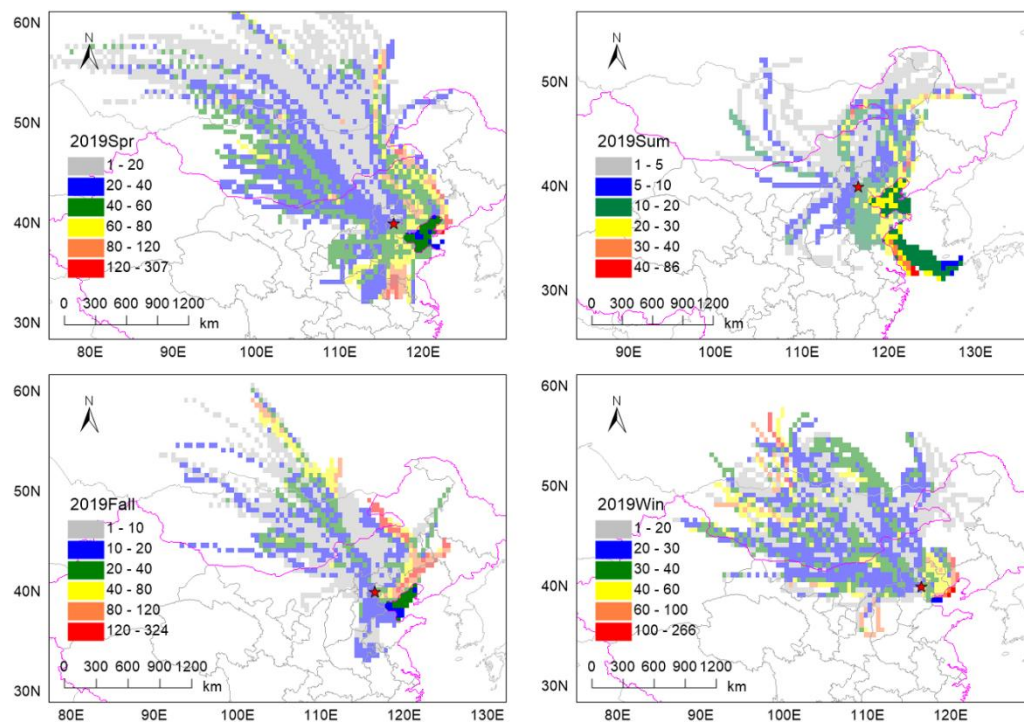
365 **Figure 4. CWT plots of potential source areas of Pb-rich particles from spring to winter, respectively.**
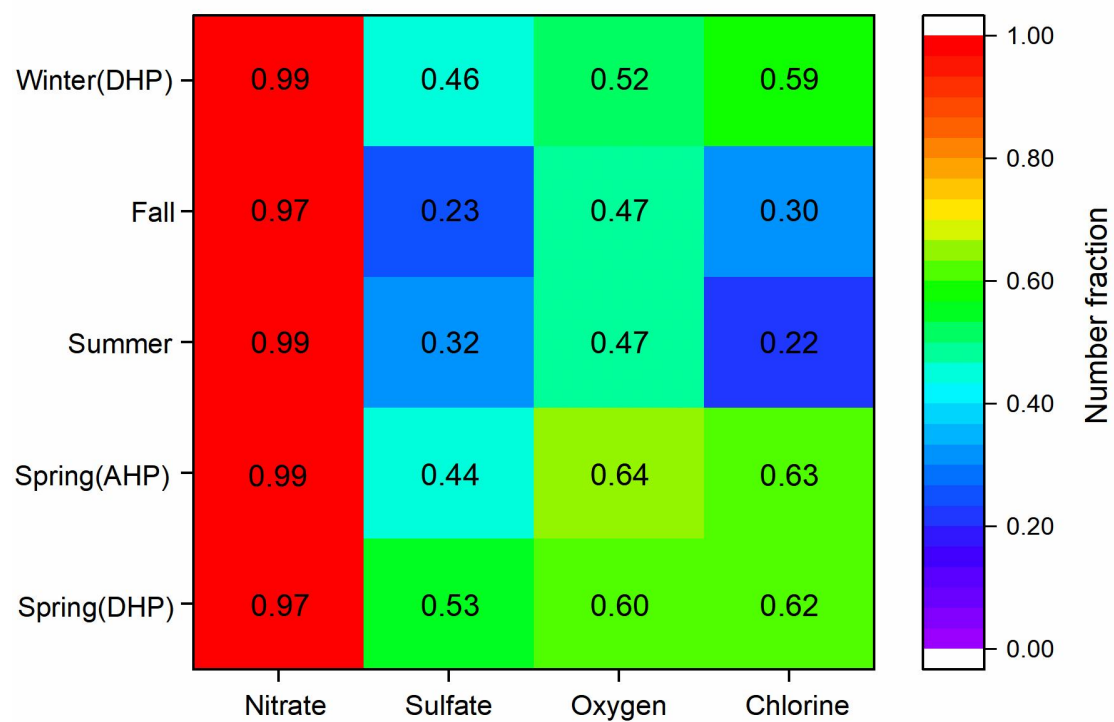
Figure 5. Number fraction of nitrate (m/z −46 [NO$_2$]$^-$ or −62 [NO$_3$]$^-$), sulfate (m/z −97 [HSO$_4$]$^-$), oxygen (m/z −16 [O]$^-$ or −17 [OH]$^-$), and chlorine (m/z −35 [^{35}Cl]$^-$ or −37 [^{37}Cl]$^-$) in Pb-rich particles from spring to winter, respectively.

370
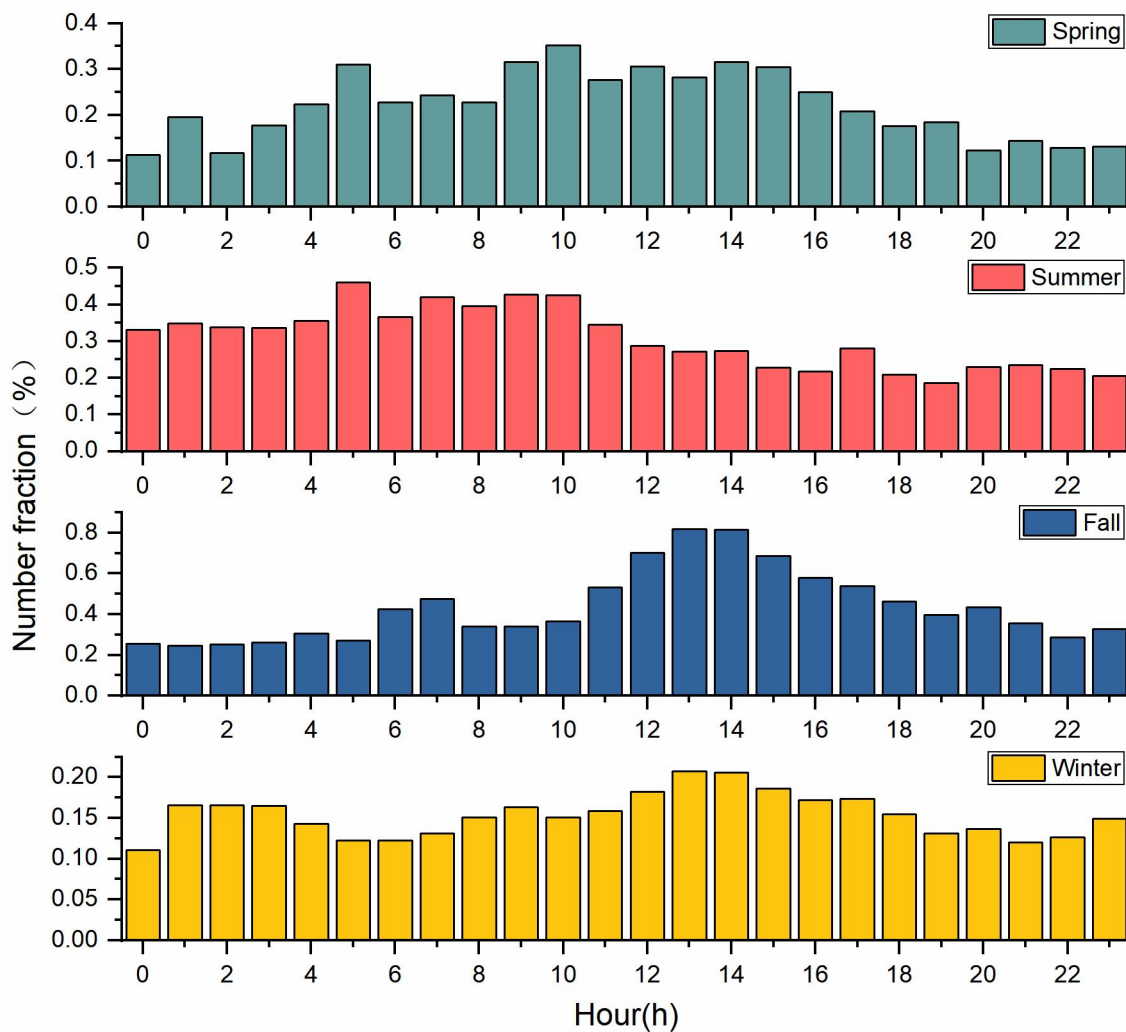
Figure 6. The diurnal variation of the number fractions of Pb-N particles in all the detected particles from spring to winter, respectively.
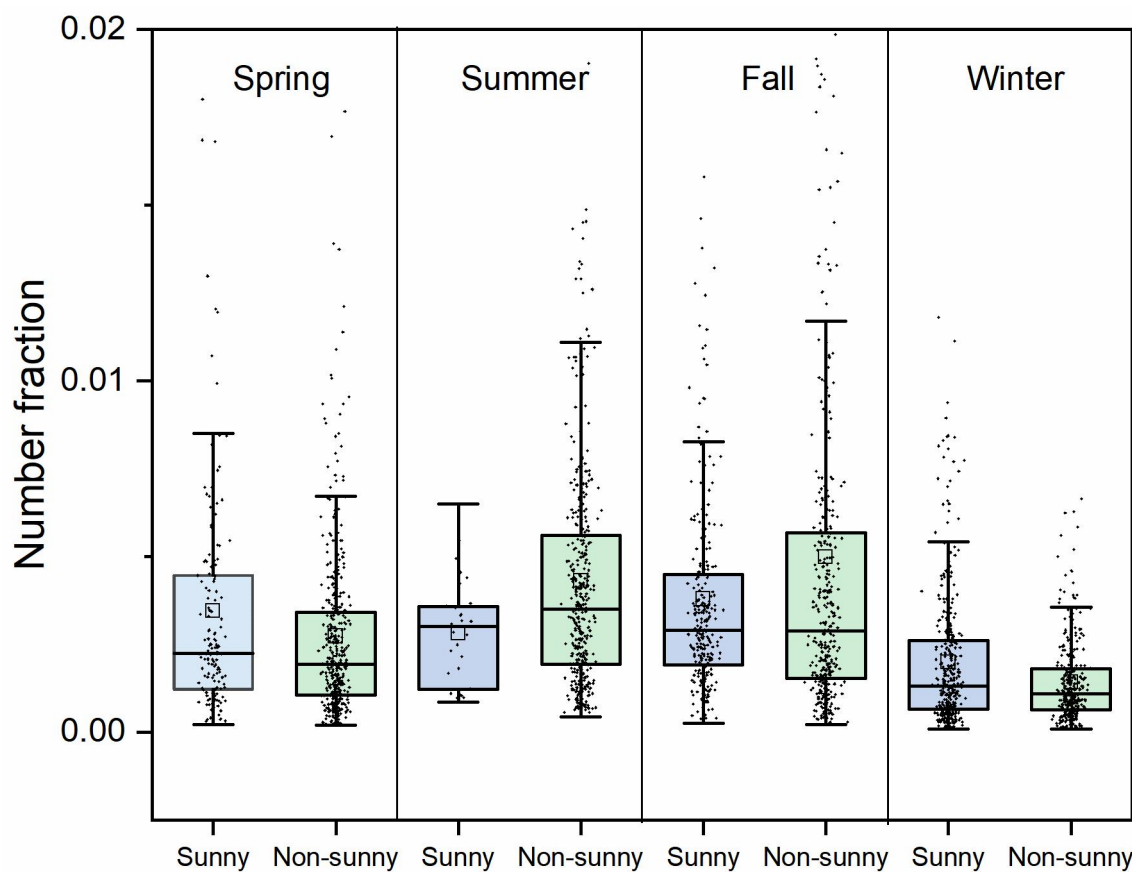
Figure 7. The number fractions of Pb-N particles in Pb-rich particles on sunny and non-sunny days during four
375   **seasons.**
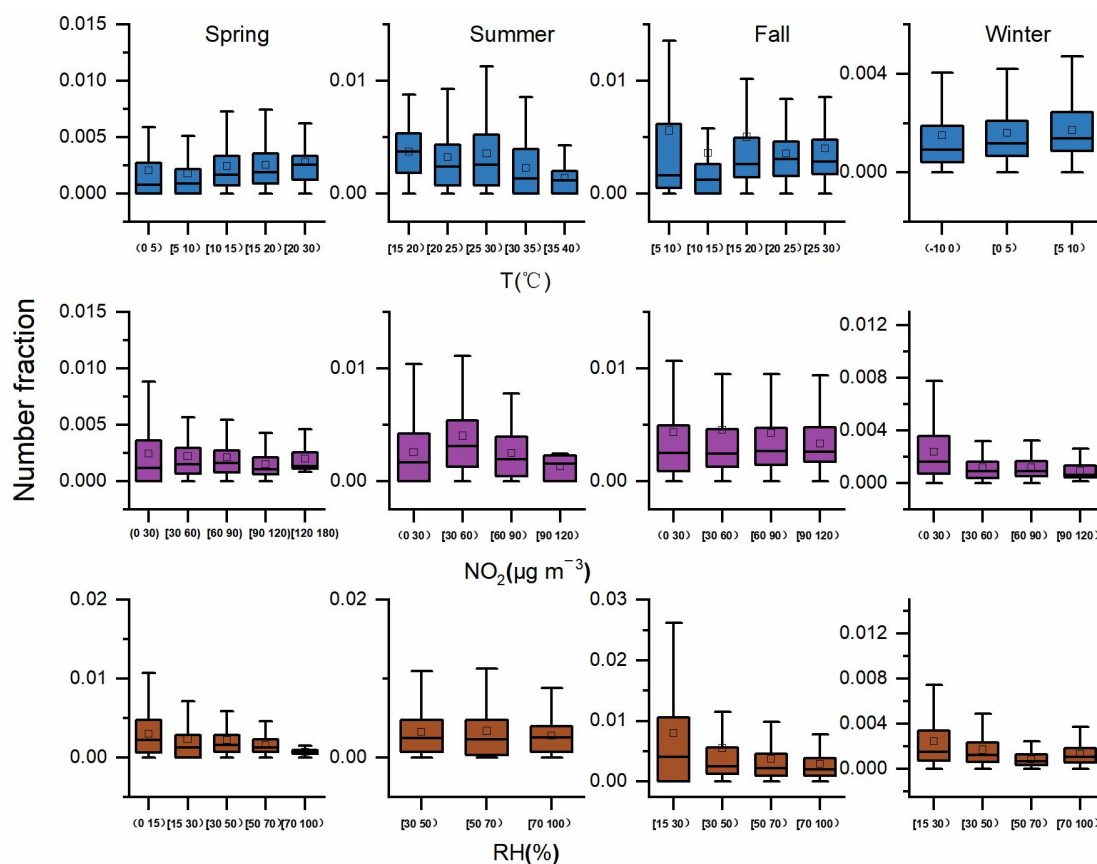
Figure 8. The relationship between T, NO₂, RH, and number fractions of Pb-N particles in Pb-rich particles from spring to winter, respectively.

Table 1 A summary of dates of SPAMS measurements, number and number fraction (Nf) of the detected Pb-rich particles.

species	Spring Number	Spring Nf(%)	Summer Number	Summer Nf(%)	Fall Number	Fall Nf(%)	Winter 2019 Number	Winter 2019 Nf(%)
All particles[a]	2058001		654094		1459253		3430337	
Pb-containing	56738	2.8%[b]	18893	2.9%[b]	43763	3.0%[b]	149590	4.4%[b]
Pb-rich	23261	1.2%[b]	8034	1.2%[b]	17930	1.2%[b]	23941	0.7%[b]
		44.5%[c]		42.5%[c]		40.9%[c]		16.0%[c]
K-Na	20004	79.2%[d]	6769	84.3%[d]	14996	83.6%[d]	18779	78.4%[d]
K-Na-Fe	1725	6.8%[d]	535	6.7%[d]	879	4.9%[d]	1270	5.3%[d]
K-Na-Cu	297	1.2%[d]	236	2.9%[d]	598	3.3%[d]	382	1.6%[d]
K-Na-Zn	231	0.9%[d]	7	0.1%[d]	32	0.2%[d]	86	0.4%[d]
K-Na-EC	1594	6.3%[d]	358	4.5%[d]	263	1.5%[d]	2128	8.9%[d]
K-OC	696	2.8%[d]	77	1.0%[d]	783	4.4%[d]	989	4.1%[d]
Others	714	2.8%[d]	52	0.6%[d]	379	2.1%[d]	307	1.3%[d]
Pb-N	4314	17.1%[e]	2292	28.5%[e]	7015	39.1%[e]	4712	19.7%[e]

[a] All particles were particles with both positive and negative spectra.
[b] Number fraction (Nf) was calculated through the number of Pb-containing or Pb-rich particles by the number of all particles over the sampling period.
[c] Number fraction (Nf) was calculated through the number of Pb-rich particles types by Pb-rich particles over the sampling period.
[d] Number fraction (Nf) was calculated through the number of Pb-rich particles by Pb-containing particles over the sampling period.
[e] Number fraction (Nf) was calculated through the number of Pb-N particles by Pb-rich particles over the sampling period.

410 **Reference**

Amann, C.A., and Siegla, D.C.: Diesel Particulates — What They Are and Why, Aerosp. Sci. Technolv., 1, 73-101, https://doi.org/10.1080/02786828208958580,1982.

Apaydin, F., Bas, H., Kalender, S., and Kalender, Y.: Subacute effects of low dose lead nitrate and mercury chloride exposure on kidney of rats, Environ. Toxicol. Phar., 41, 219-224, https://doi.org/10.1016/j.etap.2015.12.003, 2016.

415 Bas, H., and Kalender, S.: Antioxidant Status, Lipid Peroxidation and Testis-histoarchitecture Induced by Lead Nitrate and Mercury Chloride in Male Rats, Braz. Arch. Biol. Techn., 59, e16160151, https://doi.org/10.1590/1678-4324-2016160151, 2016.

Batonneau, Y., Bremard, C., Gengembre, L., Laureyns, J., Le Maguer, A., Le Maguer, D., Perdrix, E., and Sobanska, S.: Speciation of PM$_{10}$ Sources of Airborne Nonferrous Metals within the 3-km Zone of Lead/Zinc Smelters, Environ. Sci. 420 Technol., 38, 5281-5289, https://doi.org/10.1021/es0497173, 2004.

Bi, X., Zhang, G., Li, L., Wang, X., Li, M., Sheng, G., Fu, J., and Zhou, Z.: Mixing state of biomass burning particles by single particle aerosol mass spectrometer in the urban area of PRD, China, Atmos. Environ., 45, 3447-3453, https://doi.org/10.1016/j.atmosenv.2011.03.034, 2011.

Cai, J., Wang, J., Zhang, Y., Tian, H., Zhu, C., Gross, D.S., Hu, M., Hao, J., He, K., and Wang, S.: Source apportionment of 425 Pb-containing particles in Beijing during January 2013, Environ. Pollut., 226, 30-40, https://doi.org/10.1016/j.envpol.2017.04.004, 2017.

Cho, S.H., Richmond Bryant, J., Thornburg, J., Portzer, J., Vanderpool, R., Cavender, K., and Rice, J.: A literature review of concentrations and size distributions of ambient airborne Pb-containing particulate matter, Atmos. Environ., 45, 5005-5015, https://doi.org/10.1016/j.atmosenv.2011.05.009, 2011.

430 Csavina, J., Taylor, M.P., Félix, O., Rine, K.P., Eduardo Sáez, A., and Betterton, E.A.: Size-resolved dust and aerosol contaminants associated with copper and lead smelting emissions: Implications for emission management and human health, Sci. Total Environ., 493, 750-756, https://doi.org/10.1016/j.scitotenv.2014.06.031, 2014.

Cziczo, D.J., Stetzer, O., Worringen, A., Ebert, M., Weinbruch, S., Kamphus, M., Gallavardin, S.J., Curtius, J., Borrmann, S., Froyd, K.D., Mertes, S., Möhler, O., and Lohmann, U.: Inadvertent climate modification due to anthropogenic lead, Nat. 435 Geosci., 2, 333-336, https://doi.org/10.1038/ngeo499, 2009.

Draxler, R.R., and Rolph, G.D.: HYSPLIT (Hybrid Single-Particle Lagrangian Integrated Trajectory) Model access via NOAA ARL REDY Website (http://ready.arl.noaa.gov/HYSPLIT.php>), NOAA Air Resources Laboratory, Silver Spring, MD, 2003.

Duan, J., and Tan: Atmospheric heavy metals and Arsenic in China: Situation, sources and control policies, Atmos. Environ., 440 74, 93-101, https://doi.org/10.1016/j.atmosenv.2013.03.031, 2013.

Ebert, M., Worringen, A., Benker, N., Mertes, S., Weingartner, E., and Weinbruch, S.: Chemical composition and mixing-state of ice residuals sampled within mixed phase clouds, Atmos. Chem. Phys., 11, 2805-2816, https://doi.org/10.5194/acp-11-2805-2011, 2011.

Furimsky, E.: Characterization of trace element emissions from coal combustion by equilibrium calculations, Fuel Process. 445 Technol., 63, 29-44, https://doi.org/10.1016/S0378-3820(99)00067-3, 2000.

Furutani, H., Jung, J., Miura, K., Takami, A., Kato, S., Kajii, Y., and Uematsu, M.: Single-particle chemical characterization and source apportionment of iron-containing atmospheric aerosols in Asian outflow, J. Geophys. Res.-Atmos., 116, D18204, https://doi.org/10.1029/2011JD015867, 2011.

Grandjean, P., and Herz, K.T.: Trace elements as paradigms of developmental neurotoxicants: Lead, methylmercury and 450 arsenic, J. Trace Elem. Med Biol., 31, 130-134, https://doi.org/10.1016/j.jtemb.2014.07.023, 2015.

Gu, X., Qi, Y., Feng, Z., Ma, L., Gao, K., and Zhang, Y.: Lead (Pb) induced ATM-dependent mitophagy via PINK1/Parkin pathway, Toxicol. Lett., 291, 92-100, https://doi.org/10.1016/j.toxlet.2018.04.012, 2018.

Guazzotti, S., A.: Characterization of carbonaceous aerosols outflow from India and Arabia: Biomass/biofuel burning and fossil fuel combustion, J. Geophys. Res.-Atmos., 108, 1211-1222, https://doi.org/10.1029/2002JD003277, 2003.

Healy, R., Sciare, J., Poulain, L., Crippa, M., Wiedensohler, A., Prévôt, A., Sarda-Estève, B., McGuire, M., Jeong., C., McGillicuddy, E., O'Connor, I., Sodeau, G., Evans, G., and Wenger., J.: Quantitative determination of carbonaceous particle mixing state in Paris using single-particle mass spectrometer and aerosol mass spectrometer measurements. Atmos. Chem. Phys., 13, 18, 9479-9496. https://doi.org/10.5194/acp-13-9479-2013, 2013.

Hsu, Y.K., Holsen, T.M., and Hopke, P.K.: Comparison of hybrid receptor models to locate PCB sources in Chicago, Atmos. Environ., 37, 545-562, https://doi.org/10.1016/S1352-2310(02)00886-5, 2003.

Hudson, P.K., Murphy, D.M., Cziczo, D.J., Thomson, D.S., de Gouw, J.A., Warneke, C., Holloway, J., Jost, H.J., Hübler, G.: Biomass-burning particle measurements: Characteristic composition and chemical processing, J. Geophys. Res.-Atmos., 109, https://doi.org/10.1029/2003JD00, 2004.

Jakubowski, M.: Low-level environmental lead exposure and intellectual impairment in children — The current concepts of risk assessment. Int. J. Occup. Med, Environ. Health., 24, 1-7, https://doi.org/10.2478/s13382-011-0009-z, 2011.

Jeong, C., McGuire, M., Godri, K., Slowik, J., Rehbein, P., and Evans, G.: Quantification of aerosol chemical composition using continuous single particle measurements. Atmos. Chem. Phys., 11, 14, 7027-7044. https://doi.org/10.5194/acp-11-7027-2011, 2011.

Komárek, M., Ettler, V., Chrastný, V., and Mihaljevič, M.: Lead isotopes in environmental sciences: A review, Environ. Int., 34, 562-577, https://doi.org/10.1016/j.envint.2007.10.005, 2008.

Koukouzas, N., Ketikidis, C., and Itskos, G.: Heavy metal characterization of CFB-derived coal fly ash, Fuel Process. Technol., 92, 441-446, ,2011.

Kristensen, L.J.: Quantification of atmospheric lead emissions from 70 years of leaded petrol consumption in Australia, Atmos. Environ., 111, 195-201, https://doi.org/10.1016/j.atmosenv.2015.04.012, 2015.

Li, L., Huang, Z., Dong, J., Li, M., Gao, W., Nian, H., Fu, Z., Zhang, G., Bi, X., and Cheng, P.: Real time bipolar time-of-flight mass spectrometer for analyzing single aerosol particles, Int. J. Mass spectrom., 303, 118-124, https://doi.org/10.1016/j.ijms.2011.01.017, 2011.

Li, Q., Cheng, H., Zhou, T., Lin, C., and Guo, S.: The estimated atmospheric lead emissions in China, 1990–2009, Atmos. Environ., 60, 1-8, https://doi.org/10.1016/j.atmosenv.2012.06.025, 2012.

Li, Y., Zhang, H., Shao, L. M., and He, P.J.: Tracing source and migration of Pb during waste incineration using stable Pb isotopes, J. Hazard. Mater., 327, 28-34, https://doi.org/10.1016/j.jhazmat.2016.12.029, 2017.

Liang, J., and Mao, J.: Source analysis of global anthropogenic lead emissions: their quantities and species, Environ. Sci. Pollut. R., 22, 7129-7138, https://doi.org/10.1007/s11356-014-3878-4, 2015.

Liu, D.Y., Rutherford, D., Kinsey, M., and Prather, K.A.: Real-Time Monitoring of Pyrotechnically Derived Aerosol Particles in the Troposphere, Anal. Chem., 69, 1808-1814, https://doi.org/10.1021/ac9612988,1997.

Liu, Y., Xing, J., Wang, S., Fu, X., and Zheng, H.: Source-specific speciation profiles of $PM_{2.5}$ for heavy metals and their anthropogenic emissions in China, Environ. Pollut., 239, 544-553, https://doi.org/10.1016/j.envpol.2018.04.047, 2018.

Liu, Z., Chen, X., Cai, J., Baležentis, T., Li, Y., 2020. The Impact of "Coal to Gas" Policy on Air Quality: Evidence from Beijing, China, Energies, 13, 3876, https://doi.org/10.3390/en13153876, 2020.

Lu, J., Ma, L., Cheng, C., Pei, C., Chan, C.K., Bi, X., Qin, Y., Tan, H., Zhou, J., and Chen, M.: Real time analysis of lead-containing atmospheric particles in Guangzhou during wintertime using single particle aerosol mass spectrometry. Ecotoxicol, Environ. Saf., 168, 53-63, https://doi.org/10.1016/j.ecoenv.2018.10.006, 2019.

Li, L., Pan, Y.Y., Zhu, R.G., Zhang, Z.Y., Zheng, N.Z., Liu, Y.H., Liu, C., Xiao, H.W., and Xiao, H.Y.: Assessment of the

seasonal cycle of nitrate in PM₂.₅ using chemical compositions and stable nitrogen and oxygen isotopes at Nanchang, China, Atmos. Environ., 117371, https://doi.org/10.1016/j.atmosenv.2020.117371, 2020.

Moffet, R.C., Desyaterik, Y., Hopkins, R.J., Tivanski, A.V., Gilles, M.K., Wang, Y., Shutthanandan, V., Molina, L.T., Abraham, R.G., Johnson, K.S., Mugica, V., Molina, M.J., Laskin, A., and Prather, K.A.: Characterization of Aerosols Containing Zn, Pb, and Cl from an Industrial Region of Mexico City, Environ. Sci. Technol., 42, 7091-7097, https://doi.org/10.1021/es7030483, 2008.

Murphy, D.M., Hudson, P.K., Cziczo, D.J., Gallavardin, S., Froyd, K.D., Johnston, M.V., Middlebrook, A.M., Reinard, M.S., Thomson, D.S., Thornberry, T., and Wexler, A.S.: Distribution of lead in single atmospheric particles, Atmos. Chem. Phys., 7, 3195-3210, https://doi.org/10.5194/acp-7-3195-2007, 2007.

National Development and Reform Commission of China, Wintertime clean heating plan in North China (2017–2021) (2017). https://www.gov.cn/xinwen/2017-12/20/content_5248855.htm. Accessed 24 January 2025.

Oberdörster, G., Sharp, Z., Atudorei, V., Elder, A., Gelein, R., Kreyling, and W., Cox, C.: Translocation of inhaled ultrafine particles to the brain, Inhalation Toxicol., 16, 437-445, https://doi.org/10.1080/08958370490439597,2004.

Ohmsen, G.S.: Characterization of fugitive material within a primary lead smelter, J Air Waste Manag Assoc, 51, 1443-1451, https://doi.org/10.1080/10473289.2001.10464371, 2001.

Peng, L., Li, L., Lin, Q., Li, M., Zhang, G., Bi, X., Wang, X., and Sheng, G.: Does atmospheric processing produce toxic Pb-containing compounds? A case study in suburban Beijing by single particle mass spectrometry, J. Hazard. Mater., 382, 121014, https://doi.org/10.1016/j.jhazmat.2019.121014, 2020.

Rossi, E.: Low level environmental lead exposure--a continuing challenge, Clin, Biochem. Rev., 29, 63-70, http://dx.doi.org/, 2008.

Slater,E., Whalley, L., Massey, R., Ye, C., Lee, J., Squires, F., Hopkins, J, Dunmore, R.,Shaw, M., Hamilton, J., Lewis, A., Crilley, L., Kramer, L., Bloss, W., Vu, Tuan., Sun, Y., Xu, W., Yue, S., Ren, L., Acton, L., Hewitt, N., Wang, X., Fu, P., and Heard, D.: Heard1Elevated levels of OH observed in haze events during wintertime in central Beijing, Atmos. Chem. Phys., 20, 23, 14847-14871, https://doi.org/10.5194/acp-20-14847-2020, 2020.

Schindler, M., Santosh, M., Dotto, G., Silva, L.F.O., and Hochella, M.F.: A review on Pb-bearing nanoparticles, particulate matter and colloids released from mining and smelting activities, Gondwana Res., 110, 330-346, https://doi.org/10.1016/j.gr.2021.07.011, 2022.

Shtepliuk, I., Santangelo, M.F., Vagin, M., Ivanov, I.G., Khranovskyy, V., Iakimov, T., Eriksson, and J., Yakimova, R.:Understanding Graphene Response to Neutral and Charged Lead Species: Theory and Experiment, Materials, 11, 2059, https://doi.org/10.3390/ma11102059, 2018.

Sobanska, S., Ricq, N., Laboudigue, A., Guillermo, R., Brémard, C., Laureyns, J., Merlin, J.C., and Wignacourt, J.P.: Microchemical Investigations of Dust Emitted by a Lead Smelter, Environ. Sci. Technol., 33, 1334-1339, https://doi.org/10.1021/es9805270, 1999.

Sommar, J.N., Svensson, M.K., Björ, B.M., Elmståhl, S.I., Hallmans, G., Lundh, T., Schön, S.M.I., Skerfving, S., and Bergdahl, I.A.: End-stage renal disease and low level exposure to lead, cadmium and mercury; a population-based, prospective nested case-referent study in Sweden, Environ. Health., 12, 9, http://www.ehjournal.net/content/12/1/9, 2013.

Song, X.H., Hopke, P.K., Fergenson, D.P., and Prather, K.A.: Classification of Single Particles Analyzed by ATOFMS Using an Artificial Neural Network, ART-2A, Anal. Chem., 71, 860-865, https://doi.org/10.1021/ac9809682, 1999.

Song, W., Wang, Y.L., Yang, W., Sun, X.C., Tong, Y.D., Wang, X.M., Liu, C.Q., Bai, Z.P., and Liu, X.Y.: Isotopic evaluation on relative contributions of major NOₓ sources to nitrate of PM₂.₅ in Beijing, Environ. Pollut., 248, 183–190, https://doi.org/10.1016/j.envpol.2019.01.081, 2019.

Tao, Z., Guo, Q., Wei, R., Dong, X., Han, X., and Guo, Z.: Atmospheric lead pollution in a typical megacity: Evidence from

lead isotopes, Sci. Total Environ., 778, 145810, https://doi.org/10.1016/j.scitotenv.2021.145810, 2021.

Tian, H.Z., Lu, L., Hao, J.M., Gao, J.J., Cheng, K., Liu, K.Y., Qiu, P.P., and Zhu, C.Y.: A Review of Key Hazardous Trace Elements in Chinese Coals: Abundance, Occurrence, Behavior during Coal Combustion and Their Environmental Impacts, Energy & Fuels, 27, 601-614, https://doi.org/10.1021/ef3017305, 2013.

Tian, H.Z., Zhu, C.Y., Gao, J.J., Cheng, K., Hao, J.M., Wang, K., Hua, S.B., Wang, Y., and Zhou, J.R.: Quantitative assessment of atmospheric emissions of toxic heavy metals from anthropogenic sources in China: historical trend, spatial distribution, uncertainties, and control policies, Atmos. Chem. Phys., 15, 10127-10147,,2015.

Tiwari, S., Srivastava, A.K., Bisht, D.S., Parmita, P., Srivastava, M.K., Attri, S.D.: Diurnal and seasonal variations of black carbon and PM$_{2.5}$ over New Delhi, India: Influence of meteorology. Atmos. Res., 125-126, 50-62, https://doi.org/10.1016/j.atmosres.2013.01.011, 2013.

Tong, Y., Gao, J.J., Yue, T., Yuan, Y., Tang, Y., Wang, L.Q.: Tracking the flows of Hg, As, Cd, Cr, and Pb in Chinese coal-fired industrial boilers, J. Hazard. Mater., 466, 133678, https://doi.org/10.1016/j.jhazmat.2024.133678, 2024.

Wang, H.C., Lu, K.D., Chen, X.R., Zhu, Q.D., Chen, Q., Guo, S., Jiang, M.Q., Li, X., Shang, D.J., Tan, Z.F., Wu, Y.S., Wu, Z.J., Zou, Q., Zheng, Y., Zeng, L.M., Zhu, T., Hu, M. Zhang, Y.H.: High N$_2$O$_5$ concentrations observed in urban Beijing: implications of a large nitrate formation pathway. Environ. Sci. Tech. Let. 4, 416–420, DOI: 10.1021/acs.estlett.7b00341, 2017.

Wang, J., Li, Z., Ye, H., Mei, Y., Fu, J., and Li, Q.: Do China's coal-to-gas policies improve regional environmental quality? A case of Beijing, Environ. Sci. Pollut. R., 28, 57667-57685, https://doi.org/10.1007/s11356-021-14727-3, 2021.

Wang, S., Su, H., Chen, C., Tao, W., Streets, D., Lu, Z., Zheng, B., Carmichael, G., Lelieveld, J., Pöschl, U., and Cheng, Y.: Natural gas shortages during the "coal-to-gas" transition in China have caused a large redistribution of air pollution in winter 2017, Proc. Nati. Acad. Sci. U.S.A., 117, 31018-31025, https://doi.org/10.1073/pnas.2007513117, 2020.

Watson, J.G., Chen, L.W.A., Chow, J.C., Doraiswamy, P., and Lowenthal, D.H.: Source apportionment: findings from the US Supersites program, J. Air Waste Manage, 58, 265–288, https://doi.org/10.3155/1047-3289.58.2.265, 2008.

Wani, A.L., Ara, A., and Usmani, J.A.: Lead toxicity: a review, Interdiscip. Toxicol., 8, 55-64, https://doi.org/10.1515/intox-2015-0009, 2015.

Yedjou, C.G., Tchounwou, H.M., Tchounwou, P.B., 2016. DNA Damage, Cell Cycle Arrest, and Apoptosis Induction Caused by Lead in Human Leukemia Cells. Int. J. Env. Res. Public Health, 13, 56, https://doi.org/10.3390/ijerph13010056, 2016.

Yoshiie, R., Taya, Y., Ichiyanagi, T., Ueki, Y., and Naruse, I.: Emissions of particles and trace elements from coal gasification, Fuel, 108, 67-72, https://doi.org/10.1016/j.fuel.2011.06.011, 2013.

Zauscher, M., Wang, Y., Moore, M., Gaston, C., and Prather, K.: Air quality impact and physicochemical aging of biomass burning aerosols during the 2007 San Diego wildfires. Environ. Sci. Technol., 47, 14, 7633-7643. https://doi.org/10.1021/es4004137, 2013.

Zhang, Y., Wang, X., Chen, H., Yang, X., Chen, J., and Allen, J.O.: Source apportionment of lead-containing aerosol particles in Shanghai using single particle mass spectrometry, Chemosphere, 74, 501-507, https://doi.org/10.1016/j.chemosphere.2008.10.004, 2009.

Zhao, S., Chen, L., Yan, J., and Chen, H.: Characterization of lead-containing aerosol particles in Xiamen during and after Spring Festival by single-particle aerosol mass spectrometry, Sci. Total. Environ., 580, 1257-1267, https://doi.org/10.1016/j.scitotenv.2016.12.086, 2017.

Zhou, Y., Huang, X., Griffith, S., Li, M., Li, L., Zhou, Z., Wu, C., Meng, J., Chan, C., Louie, P., Yu, J.: A field measurement based scaling approach for quantification of major ions, organic carbon, and elemental carbon using a single particle aerosol mass spectrometer. Atmos. Environ., 143, 300-312. https://doi.org/10.1016/j.atmosenv.2016.08.054, 2016.